



Highly active spinel type CoCr_2O_4 catalysts for dichloromethane oxidation

Yu Wang, Ai-Pin Jia, Meng-Fei Luo, Ji-Qing Lu*

Key Laboratory of the Ministry of Education for Advanced Catalysis Materials, Institute of Physical Chemistry, Zhejiang Normal University, Jinhua 321004, China

ARTICLE INFO

Article history:

Received 25 June 2014

Received in revised form 11 October 2014

Accepted 14 October 2014

Available online 24 October 2014

Keywords:

Dichloromethane oxidation

Spinel type oxide

CoCr_2O_4 catalysts

Formate species.

ABSTRACT

A series of spinel type CoCr_2O_4 catalysts calcined at different temperatures were prepared and tested for oxidation of dichloromethane (CH_2Cl_2). These catalysts were active for this reaction. The final products in the reaction were CO_x , HCl and Cl_2 , without the formation of Cl -containing organics. The best performance was obtained on a catalyst calcined at 400 °C (CoCr_2O_4 -4), with a T_{50} of 218 °C and a T_{90} of 257 °C, which was mainly due to the highest surface area of this catalyst ($91.3 \text{ m}^2 \text{ g}^{-1}$). Detailed quantitative analyses revealed that the catalytic behavior was synergistically governed by surface acidity and reducibility of the catalyst, as evidenced by ammonia temperature-programmed desorption and hydrogen temperature-programmed reduction results, respectively. Kinetic studies revealed similar activation energies (124.5–155.5 kJ mol⁻¹) on these catalysts, implying the reaction might follow the same pathways on these catalysts. More importantly, in situ Fourier transform infrared spectroscopic investigation of the reaction revealed that formate species were the main reaction intermediates, which could be further oxidized to CO and CO_2 .

© 2014 Elsevier B.V. All rights reserved.

1. Introduction

Chlorinated volatile organic compounds (CVOCs) are associated with a broad range of industrial processes and they are recognized as a major source of air pollution [1]. The abatement of CVOCs thus becomes a very important topic in catalysis because catalytic combustion offers advantages over thermal destruction, with lower incineration temperature and higher destructive efficiency [2].

The most commonly employed catalysts for CVOCs oxidation include noble metals such as Pt [3,4], transition metal oxides such as MnO_x [5], CrO_x [6] and perovskite-type oxides [7–9], rare earth oxides such as CeO_2 [10] and zeolite [11] catalysts. Transition metal oxides catalysts are promising in practical applications because of their relatively better performance and resistance to deactivation compared to the other three type catalysts [12].

Among the transition metal oxides, Cr-based oxides are very effective for CVOCs oxidation [13–15]. Various Cr-based catalysts have been reported in literature, including $\text{CrO}_x/\text{TiO}_2$ [12,16,17], CrO_x/C [18], $\text{CrO}_x/\text{zeolites}$ [19,20] and $\text{CrO}_x\text{-CeO}_2/\text{USY}$ [21]. For example, Krishnamoorthy et al. [16] conducted oxidation of 1,2-dichlorobenzene over various supported transition metal oxides

and found that the $\text{CrO}_x/\text{TiO}_2$ was the most active catalyst compared to other TiO_2 -supported metal oxides (V_2O_5 , MoO_3 , Fe_2O_3 , and Co_3O_4), with a T_{90} (temperature when 90% conversion obtained) of about 290 °C. Moreover, Huang et al. [21] reported oxidation of various CVOCs (dichloromethane, trichloroethylene and 1,2-dichloroethane) over $\text{Cr}_2\text{O}_3\text{-CeO}_2\text{-USY}$ catalysts, and they found that T_{90} for dichloromethane, trichloroethylene and 1,2-dichloroethane were 281, 296 and 246 °C, respectively. Despite of their high activities, however, most of the supported Cr catalysts suffer severe deactivation due to the migration and/or loss of active sites during the reaction. Besides, another obstacle of the Cr catalysts for CVOCs oxidation is the formation of the extremely toxic chromium oxychloride at low temperature [22].

To overcome the disadvantages of the Cr catalysts, a possible strategy is to confine the Cr species in a robust structure, by which may suppress the transformation and leakage of Cr species during the CVOCs oxidation and hence increase the catalyst stability. In this sense, spinel type cobalt chromite oxide (CoCr_2O_4) might be a potential candidate. In such a CoCr_2O_4 structure, Co and Cr cations are bound in a solid matrix, in which the high-spin divalent Co^{2+} cations mostly occupy the tetrahedral sites, while the low-spin trivalent Cr^{3+} cations occupy the octahedral sites [23]. Indeed, the spinel type CoCr_2O_4 oxide has been widely applied in electrochromic coatings [24], protective layers [25], solar absorbers [26], gas sensors [27], electrodes for fuel cells [28], and oxidation of

* Corresponding author. Tel.: +86 579 82287325; fax: +86 579 82282595.

E-mail address: [jinqinglu@zjnu.cn](mailto:jiqinglu@zjnu.cn) (J.-Q. Lu).



different volatile organic compounds [29]. Chen et al. [29] reported methane combustion over a series of Co–Cr catalysts with different Co/Cr ratios and the best performed catalysts was a Co₁Cr₂ with a Co/Cr molar ratio of 1/2 (a spinel type CoCr₂O₄ oxide). The authors concluded that the superior performance of Co₁Cr₂ was due to the presence of high valent Cr⁶⁺ species, which caused disorders in the spinel structure of cobalt chromites and consequently enhance the adsorption of chemisorbed oxygen species. In application of CVOCs oxidation, Kim and Ihm [30] found that spinel type CoCr₂O₄ showed superior performance to other supported Cr catalysts such as CrO_x/Al₂O₃ and CrO_x/MCM-41 in total oxidation of trichloroethylene, and the authors attributed high CO₂ selectivity to the presence of abundant surface Cr³⁺ species in the CoCr₂O₄ oxide.

It can be seen that spinel type CoCr₂O₄ oxide could be promising catalyst for CVOCs oxidation; however, very limited information has been provided in literature. In addition to the development of highly active catalysts for CVOCs oxidation, some important issues such as active sites, reaction mechanisms should also be addressed in order to better understand this catalyst system. Therefore, in the current work, a series of nanocrystalline spinel type CoCr₂O₄ oxides were prepared and tested for the total oxidation of CH₂Cl₂ as a model reaction. It was found that these catalysts are very active and quite stable for the oxidation of CH₂Cl₂, and the catalytic behaviors were related to some important parameters of the catalysts such as surface acidity and reducibility. Besides, kinetic study as well as in situ infrared spectroscopic investigation provided some insights on the reaction mechanism on these catalysts.

2. Experimental

2.1. Catalyst preparation

The CoCr₂O₄ catalysts were prepared with a sol–gel method as described in a previous work [31]. In a typical procedure, 88 mmol Co(NO₃)₃·6H₂O (99.0%), 176 mmol Cr(NO₃)₃·9H₂O (99.0%) and 528 mmol citric acid (99.5%) were dissolved in 200 ml distilled water. The mixture was mildly evaporated at 90 °C until a viscous gel was obtained, which was then heated at 180 °C for 3 h. The final solid was ground and divided into four parts, followed by calcination in static air at different temperatures (400–700 °C) for 4 h. The obtained catalysts were designated as CoCr₂O_{4-x}, with x referring to calcination temperature.

2.2. Catalyst characterizations

Elemental compositions of the catalysts were determined by X-ray fluorescence (XRF) analysis, in an ARL ADVANT'X Intelli Power 4200 scanning X-ray fluorescence spectrometer. The results were analyzed using UniQuant nonstandard sample quantitative analysis software.

The BET surface areas of the catalysts were measured by N₂ adsorption at liquid-nitrogen temperature (77 K), using a surface area analyzer (Quantachrome Autosorb-1). The catalysts were pretreated at 120 °C for 6 h in vacuum.

The morphologies of the catalysts were observed by a scanning electron microscopy (SEM, Hitachi S-4800) operated at 5.0 kV.

X-ray diffraction (XRD) patterns were recorded with a PANalytical XPert PRO MPD powder diffractometer using Cu K α radiation. The working voltage was 40 kV and the working current was 40 mA. The patterns were collected in a 2θ range from 10° to 80°, with a scanning speed of 0.15° s⁻¹. Crystallite sizes and lattice parameters of the catalysts were analyzed by full-curve fitting using a JADE 6.5 software.

Raman spectra were recorded on a Renishaw RM1000 with a confocal microprobe Raman system using an excitation wavelength of 514 nm.

Hydrogen temperature-programmed reduction (H₂-TPR) technique was employed to analyze the reducibility of the catalysts. Twenty-five milligrams of the catalyst were placed in a quartz reactor and pretreated in a N₂ flow (20 ml min⁻¹) at 300 °C for 60 min in order to remove the adsorbed water and carbonates, then the sample was cooled down to 50 °C in a N₂ flow (20 ml min⁻¹). After that, the sample was heated from 50 to 900 °C with a heating rate of 10 °C min⁻¹ under a mixture of 5% H₂–95% N₂ (20 ml min⁻¹). The amount of H₂ consumption was determined by a gas chromatograph with a thermal conductivity detector (TCD), and the thermal conductively response was calibrated by the reduction of a known CuO powder sample.

The surface acidity of the catalyst was measured by ammonia temperature-programmed desorption (NH₃-TPD). Fifty milligrams of the catalyst were pretreated in a flow of N₂ (20 ml min⁻¹) at 300 °C for 0.5 h, and then was cooled down to 50 °C. Afterwards, a NH₃ flow (20 ml min⁻¹) was introduced to the sample for 15 min, followed by purging at 80 °C for 0.5 h with a N₂ flow (20 ml min⁻¹) to remove the physisorbed NH₃. Then the sample was heated from 80 to 500 °C at a rate of 10 °C min⁻¹, and the profile was recorded using a gas chromatograph (TECHTEMP GC 7890II) with a TCD detector.

X-ray photoelectron spectra of the catalysts were obtained on an ESCALAB 250Xi instrument, with a Al K α X-ray source (1486.6 eV), under about 2 × 10⁻⁹ mbar at room temperature and a pass energy of 20 eV. The binding energy (BE) of C1s core level at 284.8 eV was taken as the internal standard.

Temperature-programmed surface reaction (TPSR) was conducted on a home-made reactor connected with a mass spectrometer (MS, Qic-20 Benchtop, HidenAnalytical). Fifty milligrams of the catalyst were pretreated in a flow of air (20 ml min⁻¹) at 300 °C for 0.5 h, and then was cooled down to 50 °C. Then a flow of CH₂Cl₂/air mixture (3000 ppm CH₂Cl₂, total flow rate = 20 ml min⁻¹) was introduced to the reactor and the sample was heated from 50 to 400 °C at a rate of 10 °C min⁻¹. And *m/e* signals of 70, 44, 18, 36.5, 50.5, 49, 60 and 30 were monitored, corresponding to Cl₂, CO₂, H₂O, HCl, CH₃Cl, CH₂Cl₂, COCl₂ and HCHO, respectively. Due to the same *m/e* signals of CO and N₂ (*m/e* = 28), the formation of CO during the reaction could not be correctly identified.

In situ Fourier transform infrared (FTIR) spectra of the samples were recorded on a NEXUS670 spectrometer equipped with an MCT detector. Self-supported sample wafers (diameter = 16 mm) were prepared from 30 mg of sample by pressing at about 3 MPa. The sample was transferred to a quartz IR cell connected to the closed circulation systems and then pretreated under an air flow (90 ml min⁻¹) at 400 °C for 1 h. After the pretreatment, the sample was cooled to 50 °C and 1 ml of a gas mixture (3000 ppm CH₂Cl₂ in air) was introduced to the IR cell and the sample was heated from 50 to 400 °C at a ramp of 10 °C min⁻¹. Temperature-dependent FTIR spectra during the reaction were recorded after holding each temperature point for 10 min.

2.3. Activity test

Catalytic combustion of CH₂Cl₂ was carried out in a conventional fixed-bed reactor (i.d. = 9 mm). One gram of catalyst in 40–60 mesh was diluted into a volume of 2 ml with quartz sand, and then it was loaded in the reactor. A thermal couple was placed in the middle of the catalyst bed to monitor the reaction temperature. The CH₂Cl₂ was introduced to the reactor via passing moisture-containing air (7 ml min⁻¹) through a quartz beaker containing liquid CH₂Cl₂ kept at 0 °C, which was then

mixed with another moisture-containing air flow (493 ml min^{-1}) to the reactor. Thus, the concentration of CH_2Cl_2 was 3000 ppm (total flow rate = 500 ml min^{-1} with a total water vapor concentration of about 12000 ppm, GHSV = 15000 h^{-1}). The conversion of CH_2Cl_2 was analyzed by a gas chromatograph (Shimadzu, GC-14C) equipped with an FID detector. The outlet reaction mixture was neutralized by passing through a 0.1 M NaOH aqueous solution.

Conversion of CH_2Cl_2 was calculated as follows:

$$X_{\text{CH}_2\text{Cl}_2} = \frac{[\text{CH}_2\text{Cl}_2]_{\text{in}} \text{vol.\%} - [\text{CH}_2\text{Cl}_2]_{\text{out}} \text{vol.\%}}{[\text{CH}_2\text{Cl}_2]_{\text{in}} \text{vol.\%}}$$

where $[\text{CH}_2\text{Cl}_2]_{\text{in}}$ and $[\text{CH}_2\text{Cl}_2]_{\text{out}}$ were the CH_2Cl_2 concentrations in the inlet and outlet gas (vol.%), respectively.

The kinetic study was performed on the same fixed bed reactor of the catalytic CH_2Cl_2 oxidation as mentioned above. The feed gases were measured with mass flow controllers and mixed prior to the reactor inlet. For kinetic measurements, the reactor was operated in a differential mode with the CH_2Cl_2 conversion less than 15%. 0.5 g catalyst in 40–60 mesh was diluted with quartz sand to a volume of 2 ml and the reaction conditions were the same as in the above-mentioned fixed-bed testing (CH_2Cl_2 concentration was 3000 ppm, total flow rate was 500 ml min^{-1}). Also, the absence of mass transport resistances was checked by Weisz–Prater criterion for internal diffusion and Mears' criterion for external diffusion and the absence of heat transfer was checked by Mears' criterion [32] (See Supplementary Information for detailed calculation). For example, on the CoCr_2O_4 -4 catalyst, the calculated values under kinetic conditions are 2.22×10^{-3} for the Weisz–Prater criterion for internal diffusion, 1.19×10^{-2} for the Mears' criterion for external diffusion and 9.5×10^{-3} for the Mears' criterion for heat transfer. Those results ensure plug-flow and isothermal conditions within the catalyst bed.

Table 1
Physical properties of spinel CoCr_2O_4 catalysts.

| Catalyst | $S_{\text{BET}} (\text{m}^2 \text{ g}^{-1})$ | Cell parameter (nm) | Average crystallite size (nm) |
|------------------------------|--|---------------------|-------------------------------|
| CoCr_2O_4 -4 | 91.3 | 0.8314 | 12.8 |
| CoCr_2O_4 -5 | 51.9 | 0.8316 | 17.7 |
| CoCr_2O_4 -6 | 23.2 | 0.8324 | 27.4 |
| CoCr_2O_4 -7 | 6.1 | 0.8350 | 30.7 |

3. Results and discussion

3.1. Catalyst characterizations

The bulk compositions of Co and Cr elements in the CoCr_2O_4 catalysts are 25.3 and 44.4 wt.%, respectively, as determined by XRF. These values correspond to a Co/Cr molar ratio of 1/2. The surface areas of the catalysts listed in Table 1 decline dramatically with calcination temperature, with the sample calcined at 400°C (CoCr_2O_4 -4) having a surface area of $91.3 \text{ m}^2 \text{ g}^{-1}$ while the sample calcined at 700°C (CoCr_2O_4 -7) having a surface area of $6.1 \text{ m}^2 \text{ g}^{-1}$. The decline in surface area is due to the sintering of crystallites during the high temperature calcination.

SEM images of the CoCr_2O_4 catalysts are shown in Fig. 1. It can be seen that all these samples consist of nano-sized aggregates and no obvious porous structures are detected.

Fig. 2a presents the XRD patterns of the CoCr_2O_4 catalysts. All the samples show characteristic diffraction peaks of cubic phase CoCr_2O_4 spinel (JCPDS 22-1084) and no other diffraction peaks are detected. Moreover, with increasing calcination temperature, the peaks become more intense. Accordingly, the average crystallite size significantly increase with calcination temperature, ranging from 12.8 nm for the CoCr_2O_4 -4 to 30.7 nm for the CoCr_2O_4 -7 (Table 1). The growth of the crystallite is in agreement of the decline of surface area. In addition, a slight shift of the diffraction peaks toward lower degrees is observed with increasing

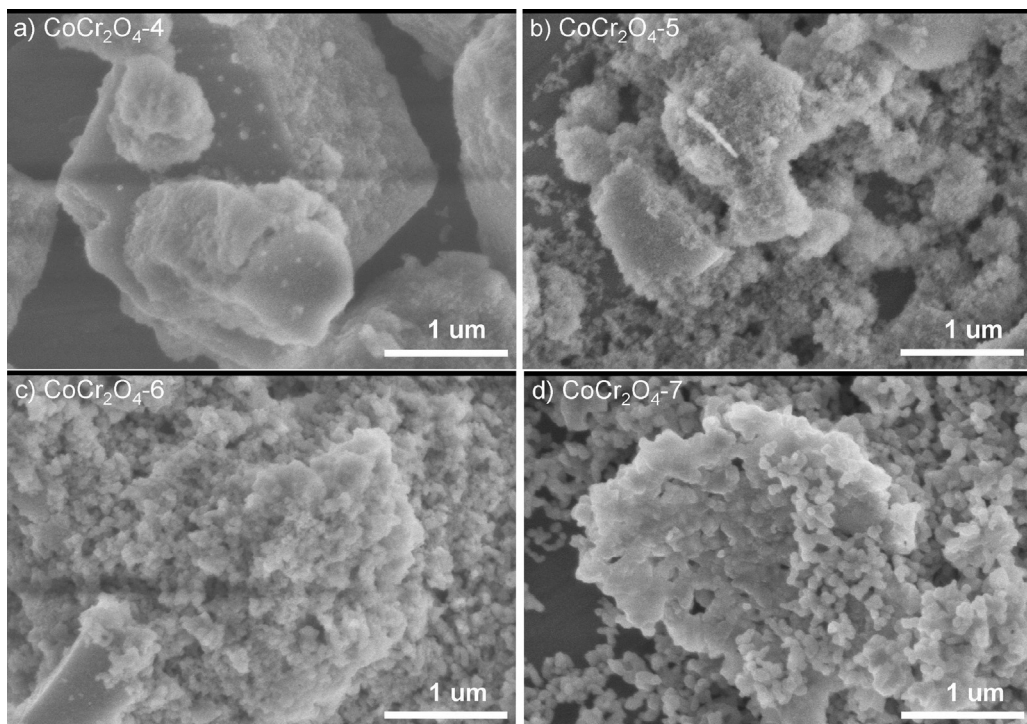


Fig. 1. SEM images of (a) CoCr_2O_4 -4, (b) CoCr_2O_4 -5, (c) CoCr_2O_4 -6 and (d) CoCr_2O_4 -7 catalysts.

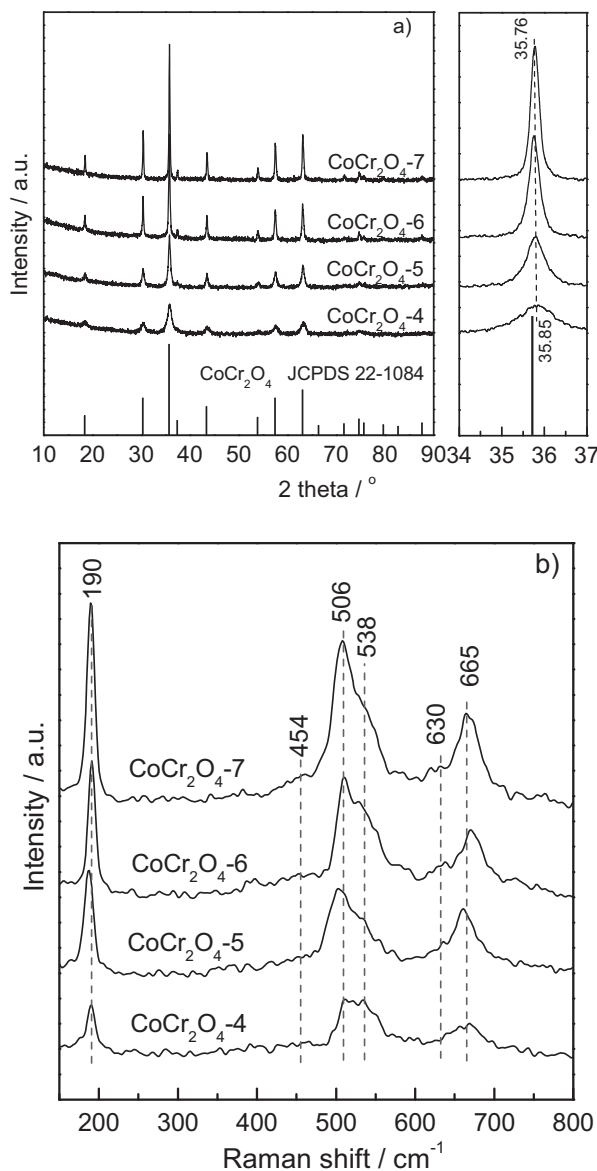


Fig. 2. (a) XRD patterns and (b) Raman spectra of spinel CoCr₂O₄ catalysts.

calcination temperature, which consequently results in an increasing cell parameter of the sample (**Table 1**). The variation of lattice parameters could be due to the disordering of the cations in the spinel structures. At low-temperature calcination, Co³⁺ ions could partially replace Cr³⁺ in the oxide, which leads to a decline of lattice parameter because the ionic radius of the six-coordinated Co³⁺ in low-spin configuration (0.0545 nm) is smaller than that of the six-coordinated Cr³⁺ (0.0615 nm) [33]. However, when the sample was calcined at high temperature (e.g. 700 °C), the disordering of the cations in the spinel structure becomes less intense, which leads to a larger lattice parameter.

Raman spectra of the samples are shown in **Fig. 2b**. All these samples show four distinct bands at 190, 506, 538 and 665 cm⁻¹, as well as two weak bands at 454 and 630 cm⁻¹. According to group theory, CoCr₂O₄ with purely normal spinel structure has five Raman-active phonon modes ($\Gamma = 1A_{1g} + 1E_g + 3F_{2g}$) [34,35]. All of these modes can be observed at approximately 190 cm⁻¹ (F_{2g}), 454 cm⁻¹ (E_g), 506 cm⁻¹ (F_{2g}), 538 cm⁻¹ (unclear mode), 630 cm⁻¹ (F_{2g}), and 665 cm⁻¹ (A_{1g}). The Raman spectra are similar as those reported in literature [36]. In addition, Chen et al. [36] attributed the band at 538 cm⁻¹ to a Raman-active mode which is due to the

Table 2
Surface compositions of spinel CoCr₂O₄ catalysts.

| Catalyst | Atomic ratio | | | |
|-------------------------------------|-------------------------------------|-------------------------------------|-------------------------------------|------------------------------------|
| | Co ³⁺ /Co _{tot} | Cr ³⁺ /Cr _{tot} | Cr ⁶⁺ /Cr _{tot} | O _{ads} /O _{lat} |
| CoCr ₂ O ₄ -4 | 0.23 | 0.81 | 0.19 | 0.57 |
| CoCr ₂ O ₄ -5 | 0.20 | 0.80 | 0.20 | 0.53 |
| CoCr ₂ O ₄ -6 | 0.17 | 0.81 | 0.19 | 0.52 |
| CoCr ₂ O ₄ -7 | 0.15 | 0.81 | 0.19 | 0.50 |

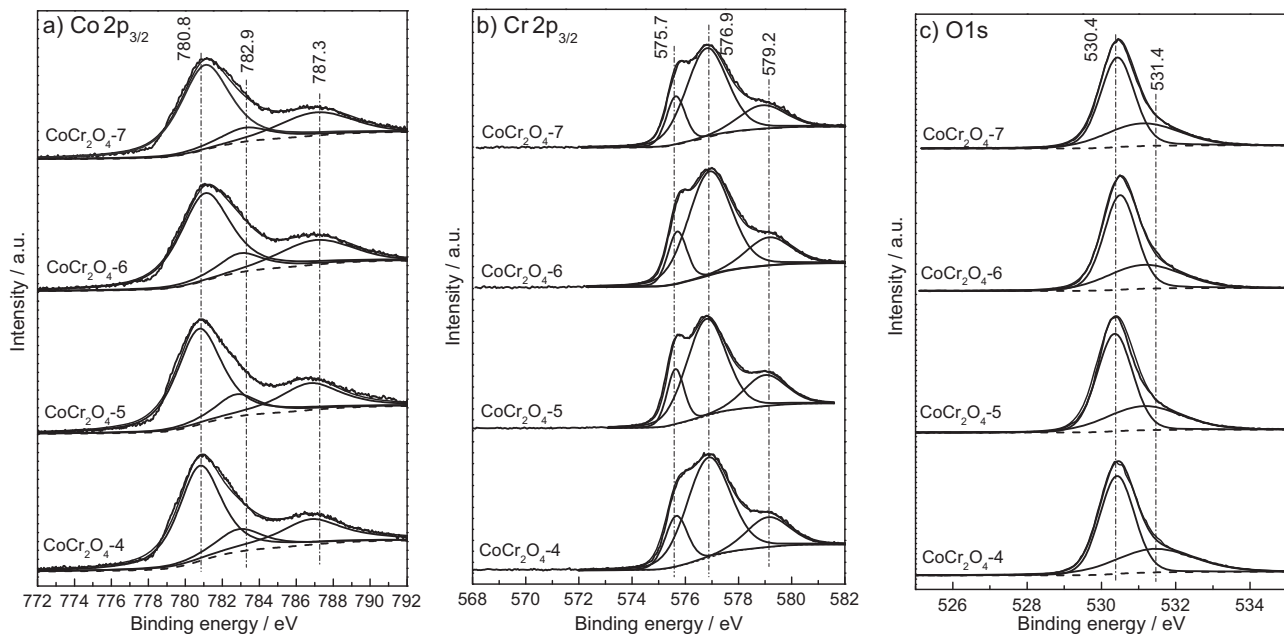
cation disordering that induces a breakdown of the translation symmetry. Moreover, it is found that the intensities of the bands at 190, 506, and 665 cm⁻¹ gradually increase with increasing calcination temperatures. Such trends are due to the changes either in electronic properties [36] or the crystallite sizes [37,38] of the CoCr₂O₄ oxides.

The oxidation states of the elements in the catalysts and surface compositions are analyzed by XPS, as shown in **Fig. 3** and **Table 2**. For the Co 2p_{3/2} spectra (**Fig. 3a**), a broad and overlapped band at binding energies (BEs) of 772–794 eV is observed in all samples, which could be further deconvoluted into three components with BEs centered at 780.8, 782.9 and 787.3 eV. The peaks with BEs at 780.8 and 782.9 eV could be assigned to Co²⁺ and Co³⁺, respectively [39–41]. And the presence of Co²⁺ in the catalysts is also confirmed by the satellite peak at 787.3 eV [36]. The surface composition analyses also indicate that the concentration of Co³⁺ cations progressively decreases with increasing calcination temperature (23% Co³⁺ in the CoCr₂O₄-4 and 15% in the CoCr₂O₄-7, **Table 2**), which suggests that calcination temperature exerts influences on the oxidation states of the Co species in the samples. The higher Co³⁺ content in the low-temperature calcined sample (e.g. CoCr₂O₄-4) implies that some of these Co³⁺ cations could replace Cr³⁺ cations in the B site of the AB₂O₄ spinel structure, which is consistent with the smaller lattice parameter in the CoCr₂O₄-4 sample (**Table 1**).

In **Fig. 3b**, the peak of Cr 2p_{3/2} could also be resolved into three components at BEs at 575.7, 576.9 and 579.2, assigning to Cr(OH)₃ or Cr₂O₃ [42], Cr³⁺ (occupied octahedral sites) [29,43,44] and Cr⁶⁺ [30,45], respectively. The occupied octahedral Cr³⁺ sites are exposed at the surface of the spinel samples and regarded as active sites for the oxidation reaction [29,43,44]. The presence of Cr⁶⁺ in spinel CoCr₂O₄ oxides was reported by Słoczyński et al. [45], as the authors found that surface of Cr-containing spinel oxides was enriched with Cr⁶⁺, and the location of Cr⁶⁺ was surface-only. Besides, Kim and Ihm [30] found that the Cr⁶⁺ was stable on the surface in H₂ environment and was inactive for the TCE oxidation. Surface compositions of the Cr species in the catalysts (**Table 2**) reveal that the concentrations of various Cr species in these catalysts remain almost constant regardless of the calcination temperature.

As for the O1s spectra (**Fig. 3c**), the asymmetric peak could be deconvoluted to one main peak at BE of 530.4 eV and one weak peak at BE of 531.4 eV, which could be assigned to lattice oxygen (O_{latt}) and adsorbed oxygen (O_{ads}), respectively [46]. The O_{ads} peaks can be associated with a wide variety of species such as surface chemisorbed oxygen, hydroxyl and oxygen ions in low coordination situation and oxygen-containing surface contamination [47]. Moreover, the areal ratio of O_{ads}/O_{latt} reflects the proportion of the two different oxygen species, and a higher ratio indicates larger amount of chemisorbed oxygen species [48]. As shown in **Table 2**, the O_{ads}/O_{latt} ratio is relatively higher on the CoCr₂O₄-4 catalyst compared to those on the other catalysts, implying higher amount of surface oxygen on the CoCr₂O₄-4 catalyst.

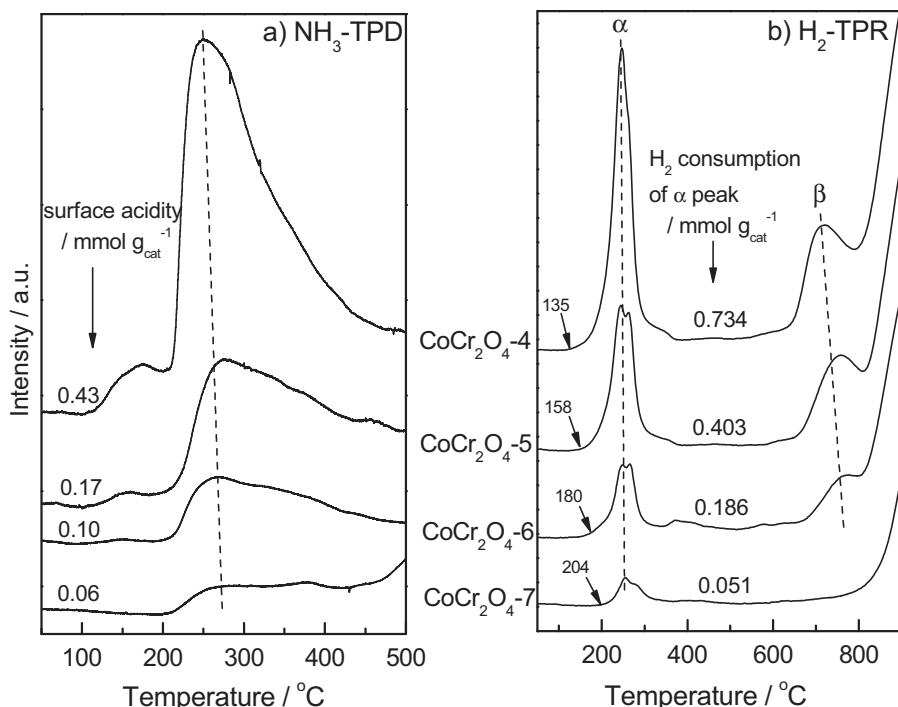
Surface acidity plays an important role in CVOCs oxidation as they provide sites for the chemisorption of CVOCs molecules [3]. Thus, surface acidities of the catalysts are measured by NH₃-TPD,

Fig. 3. Co₂p, Cr₂p and O₁s XPS spectra of spinel CoCr₂O₄ catalyst.

and the results are shown in Fig. 4a. One weak peak at less than 200 °C and an intense peak at about 210–260 °C are detected in the catalysts, indicating the presence of surface acidic sites in the catalysts. The amounts of NH₃ desorption on these samples are also quantified, which are 0.43, 0.17, 0.10 and 0.06 mmol g_{cat}⁻¹ for the CoCr₂O₄-4, CoCr₂O₄-5, CoCr₂O₄-6 and CoCr₂O₄-7, respectively. The declined values clearly suggest that calcination temperature could remarkably influence the surface acidity of the cobalt chromites [49]. However, considering that the surface areas of these catalysts are very different, and the amount of surface acidic sites should be normalized based on surface area. It is found that

the normalized values of the catalysts are essentially constant (4.28–4.92 μmol m⁻²).

Reducibility of the catalysts is measured by H₂-TPR technique, as shown in Fig. 4b. There are two reduction peaks at about 250 °C (α peak) and 750 °C (β peak), which are attributed to the reduction of surface Cr⁶⁺ to Cr³⁺ species [31] and reduction of Cr³⁺ to lower oxidation states [29], respectively. The H₂ consumptions of the α peak of the catalysts are calculated to be 0.734, 0.403, 0.186 and 0.051 mmol g_{cat}⁻¹ for the CoCr₂O₄-4, CoCr₂O₄-5, CoCr₂O₄-6 and CoCr₂O₄-7 catalysts, respectively. Note that the nominal H₂ consumption of the catalyst is about 2.04 mmol g_{cat}⁻¹ if we assume the

Fig. 4. (a) NH₃-TPD and (b) H₂-TPR profiles of spinel CoCr₂O₄ catalysts.

Cr^{6+} contents in these catalysts are about $1.76 \text{ mmol g}_{\text{cat}}^{-1}$ based on the XPS results (Table 2). Thus, the actual H_2 consumption values ($0.734\text{--}0.051 \text{ mmol g}_{\text{cat}}^{-1}$) are much lower than the nominal ones, indicating that only partial Cr^{6+} cations could be reduced. Moreover, the higher H_2 consumption of the $\text{CoCr}_2\text{O}_4\text{-}4$ suggests more facile reduction of the low-temperature calcined sample probably because of its smaller nano-crystallites compared to others [50] even though the compositions of these catalysts are the same. The easier reduction of the $\text{CoCr}_2\text{O}_4\text{-}4$ sample is also verified by the fact that the onset temperature of the α peak is much lower on the $\text{CoCr}_2\text{O}_4\text{-}4$ (135°C) compared to $\text{CoCr}_2\text{O}_4\text{-}7$ (204°C). The assignment of the α peak to the reduction of surface species is also evidenced by an analysis method of the TPR results developed by Zimmer et al. [51]. The authors proposed an equation:

$$\frac{N_{\text{total}}}{M_{\text{sample}}} = a + b \times \frac{A_{\text{sample}}}{M_{\text{sample}}}$$

where N_{total} is the H_2 consumption of one certain peak, M_{sample} is the weight of the sample, A_{sample} is the surface area of the sample, and a and b are constants. If $N_{\text{total}}/M_{\text{sample}}$ is plotted against $A_{\text{sample}}/M_{\text{sample}}$ and a linear correlation could be established, then it could be concluded that the certain peak is due to the reduction of the surface. In the current work, the H_2 consumptions of α peak in these samples are plotted according to above equation. A perfect linear regression of the data yields an intercept $a = 5.84 \mu\text{mol m}^{-2}$ and a slope $b = 7.79 \mu\text{mol m}^{-2}$ (see Fig. S1 in Supplementary Information), which indicates that the α peak in Fig. 4b is dominated by the reduction of the surface Cr^{6+} species.

3.2. Catalytic testing

The catalytic activities of the catalysts for CH_2Cl_2 oxidation are measured as a function of the reaction temperature and the light-off curves are shown in Fig. 5a. The overall activities follow the order of $\text{CoCr}_2\text{O}_4\text{-}4 > \text{CoCr}_2\text{O}_4\text{-}5 > \text{CoCr}_2\text{O}_4\text{-}6 > \text{CoCr}_2\text{O}_4\text{-}7$. To better compare the activities of these catalysts, T_{50} (the temperature at which a conversion of 50% is obtained) values are also listed in Fig. 5a. The T_{50} values are 217 , 231 , 259 and 278°C for the $\text{CoCr}_2\text{O}_4\text{-}4$, $\text{CoCr}_2\text{O}_4\text{-}5$, $\text{CoCr}_2\text{O}_4\text{-}6$ and $\text{CoCr}_2\text{O}_4\text{-}7$, respectively. It is worth pointing out that the spinel CoCr_2O_4 catalysts in the current work are very active for CH_2Cl_2 oxidation, and these catalysts are superior to other reported catalyst systems such as CrO_3/C [52], $\text{Mn}/\text{HZSM-5}$ [53], Pd/CrZr [54], CrAlO [55] and $\text{K-Pt}/\text{Al}_2\text{O}_3$ [4] (see Table S1 in Supplementary Information). For example, the reaction rate on the $\text{CoCr}_2\text{O}_4\text{-}4$ catalyst at 250°C is $3.897 \text{ mmol}_{\text{CH}_2\text{Cl}_2} \text{ g}_{\text{cat}}^{-1} \text{ h}^{-1}$, which is much higher than the rate obtained on a 18CrAlO catalyst ($0.241 \text{ mmol}_{\text{CH}_2\text{Cl}_2} \text{ g}_{\text{cat}}^{-1} \text{ h}^{-1}$) reported in our previous work [55].

It should be noticed that for CVOCS oxidation, high conversion is not the only criterion for good catalyst systems, and selectivities of the products are more important. The desired products in Cl-containing CVOCS oxidation should be CO_2 and HCl or Cl_2 . Therefore, TPSR over the catalysts were carried out and the product distributions are also analyzed on these spinel catalysts by MS, and the results are shown in Fig. 5b. As shown in Fig. 5b, the detectable final products over the $\text{CoCr}_2\text{O}_4\text{-}4$ and $\text{CoCr}_2\text{O}_4\text{-}7$ catalysts are CO_2 , HCl , Cl_2 , as well as very small amount of HCHO . No other Cl-containing organic compounds are detected. The product distributions are quite different from those obtained on Al_2O_3 -based catalysts, on which Cl-containing organic compounds such as CH_3Cl are always formed [56]. However, the formation of CO during the reaction could not be ruled out because of its same m/e signal ($m/e = 28$) as that of N_2 . Besides, it can be seen that the onset temperatures of the two catalysts are different (260°C for the $\text{CoCr}_2\text{O}_4\text{-}4$ and 300°C for the $\text{CoCr}_2\text{O}_4\text{-}7$), and concentrations of the products are much larger on the $\text{CoCr}_2\text{O}_4\text{-}4$ compared to those on the $\text{CoCr}_2\text{O}_4\text{-}7$, judging from the peak areas of the products. These

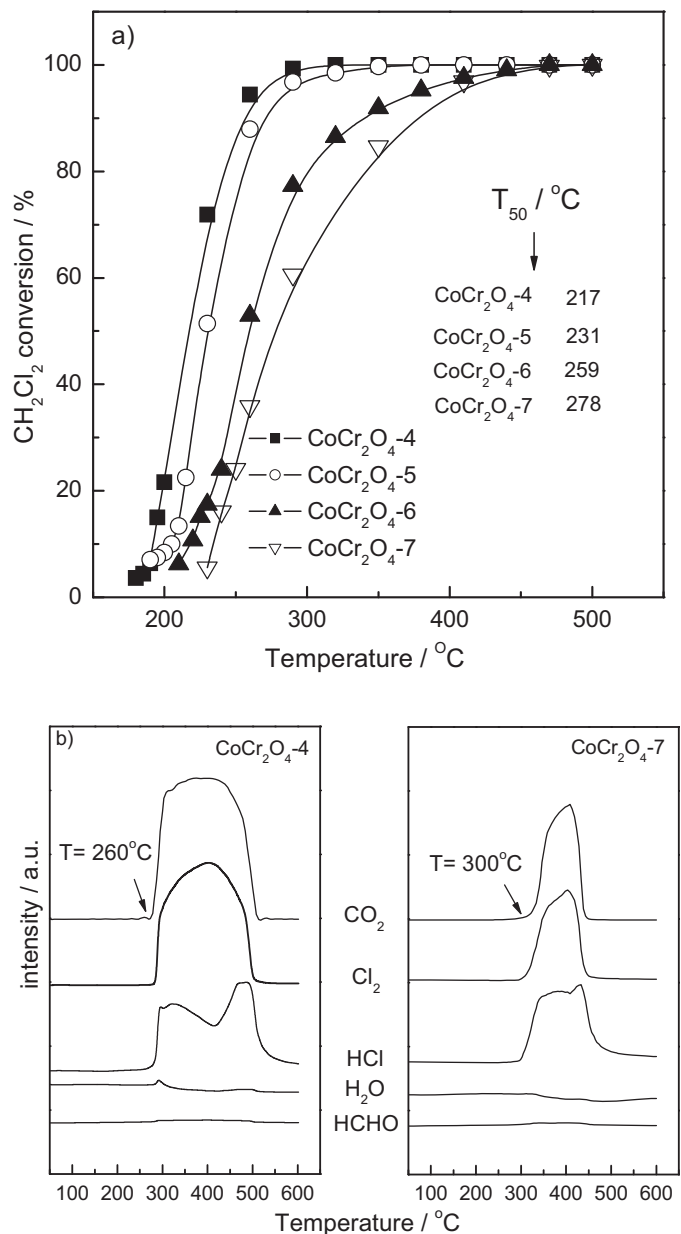


Fig. 5. (a) Light-off curves and (b) product distributions of CH_2Cl_2 oxidation over $\text{CoCr}_2\text{O}_4\text{-}4$ and $\text{CoCr}_2\text{O}_4\text{-}7$ catalysts.

results again confirm that the $\text{CoCr}_2\text{O}_4\text{-}4$ catalyst is more active than the $\text{CoCr}_2\text{O}_4\text{-}7$.

The stability of the catalysts is also investigated. As can be seen in Fig. 6, the catalysts are quite stable during 10 h reaction. Note that in order to obtain similar CH_2Cl_2 conversions (about 80–90%) over these catalysts, different reaction temperatures were used (for the $\text{CoCr}_2\text{O}_4\text{-}4$ and $\text{CoCr}_2\text{O}_4\text{-}5$ the reaction temperature was 250°C , while for the $\text{CoCr}_2\text{O}_4\text{-}6$ and $\text{CoCr}_2\text{O}_4\text{-}7$ the reaction temperature was 350°C). The bulk compositions and surface areas of the spent catalysts are very close to those of the fresh samples. For example, the spent $\text{CoCr}_2\text{O}_4\text{-}4$ has a surface area of $93.1 \text{ m}^2 \text{ g}^{-1}$ and a Cr content of 44.2 wt.%, which are close to the values of the fresh $\text{CoCr}_2\text{O}_4\text{-}4$. Moreover, comparison of the catalysts properties (XRD and XPS results) before and after reaction reveals that the catalysts remain unchanged after reaction (see Figs. S2 and S3 and Table S2 in Supplementary Information). The stable CoCr_2O_4 catalysts are also probably related to the spinel structure, in which the Co and Cr species are confined in a relatively robust matrix. Another

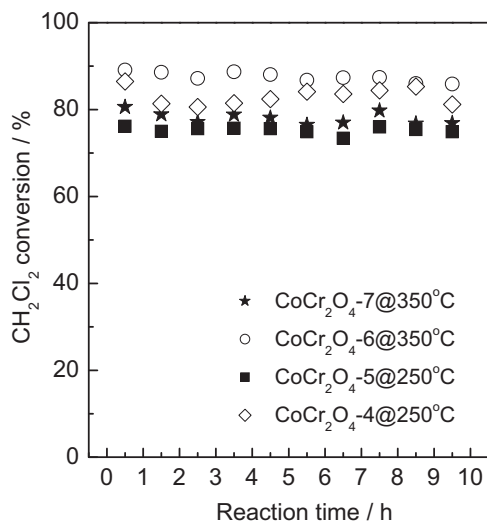


Fig. 6. Stability of spinel CoCr₂O₄ catalysts at different reaction temperatures.

noteworthy point is the possible formation of toxic chromium oxychloride such as Cr(ClO)₂ during the reaction. In the current work, since the Cr content and the physical/chemical properties of the spent sample do not change, it is quite safe to conclude that there is no such chromium oxychloride formed during the reaction. Besides, chromium oxychloride has a color of dark red, which has not been observed in the current work.

It is generally recognized that surface acidity and catalyst reducibility are two important parameters for CVOCs oxidation because the surface acidic sites provide centers for CVOCs molecule chemisorption, while the enhanced reducibility of the catalyst is beneficial to the activation of oxygen species and lattice oxygen of the oxides could often directly participate in the reaction [3]. The activity of the catalyst is usually determined by synergistic effects of these two parameters [4,10]. Thus, relationship between catalyst reducibility, surface acidity and catalytic performance is plotted as shown in Fig. 7. As shown in Fig. 7a, the specific reaction rate in unit of $\mu\text{mol g}_{\text{cat}}^{-1} \text{s}^{-1}$ (data taken from

Fig. 5a at the reaction temperature of 230°C) is proportional to both the surface acidic sites (data taken from Fig. 4a) and the surface reducibility (data taken from Fig. 4b), which strongly suggests that the overall activity of the catalyst is directly related to these two parameters. However, considering that these catalysts have very different surface areas, these variables (reducibility, surface acidity and reaction rate) should be normalized based on surface area, and the correlation is shown in Fig. 7b. It is found that the areal reaction rates are essentially constant, ranging from $0.82\text{--}1.09 \times 10^{-8} \text{ mol m}^{-2} \text{ s}^{-1}$. These rates are in agreement with the essentially constant surface acidity ($4.31\text{--}4.92 \text{ mmol NH}_3 \text{ m}^{-2}$) and reducibility ($7.76\text{--}8.04 \text{ mmol H}_2 \text{ m}^{-2}$). These results indicate that the enhanced activity of the CoCr₂O₄-4 is mainly due to its higher surface area, as the catalyst with high surface area certainly contains more active sites compared to that with low surface area.

3.3. Mechanistic investigation

For spinel type oxides (AB₂O₄) in catalytic reactions, it is recognized that the octahedral B-site cations are the active sites because these cations are exposed at the surface while the tetrahedral A-site cations are usually inactive [29,43]. In the case of CoCr₂O₄ system, Cr species in B site play very essential roles in the reaction, as reported in previous work [30]. In the current work, the Cr species in the CoCr₂O₄ catalysts provide surface acidic sites for CH₂Cl₂ chemisorption and active oxygen species (either adsorbed oxygen or lattice oxygen) as confirmed by the NH₃-TPD (Fig. 4a) and H₂-TPR (Fig. 4b) results, which are two important parameters governing the catalytic activity.

Since the CoCr₂O₄ catalysts employed in the current work have very different activities, it is possible that reaction pathways might differ on these catalysts. To clarify this point, kinetic studies were performed on these catalysts and the Arrhenius plots are shown in Fig. 8. Note that the CH₂Cl₂ conversions are low (typically less than 20%) to ensure a differential reaction mode on the catalyst (see Table S3 for the detailed reaction rates and the verification of the absence of mass and heat transfer limits in Supplementary Information). It is found that the apparent activation energies obtained on these catalysts are 124.5–155.5 kJ mol⁻¹, which are comparable

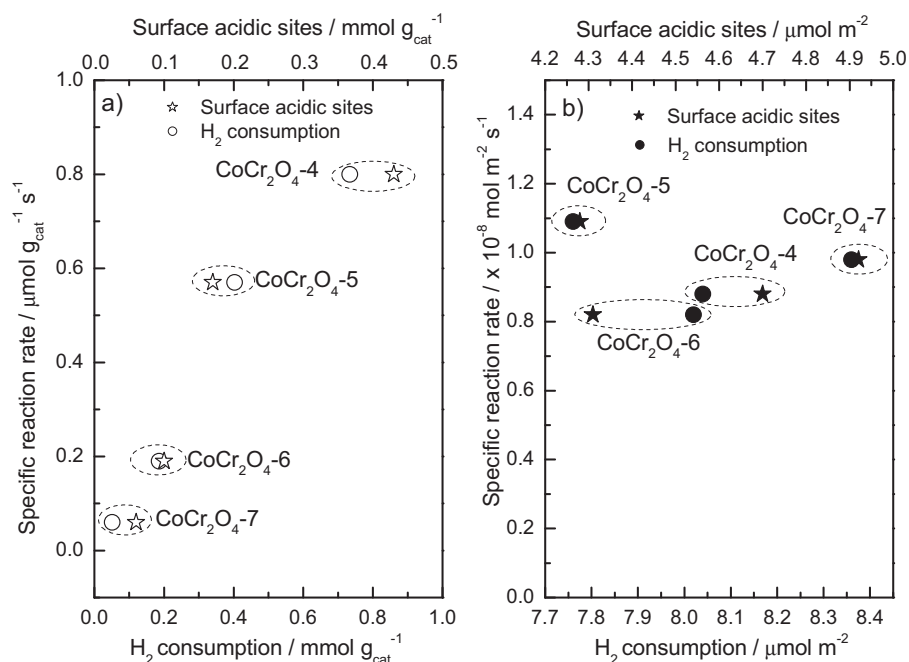


Fig. 7. Correlation between (a) overall and (b) normalized surface acidity, catalyst reducibility and specific reaction rate of CoCr₂O₄ catalysts.

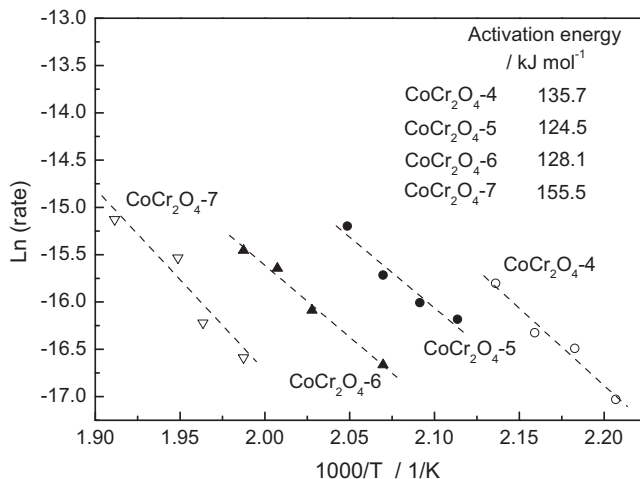


Fig. 8. Arrhenius plots of CH_2Cl_2 oxidation over spinel CoCr_2O_4 catalysts.

to the values reported on $\text{Pt}/\text{Al}_2\text{O}_3$ catalysts [4]. The similar activation energies on these spinel catalysts suggest that the reaction pathways are likely unchanged in spite of their different overall activities.

In order to further understand the catalytic behaviors of these CoCr_2O_4 catalysts, in situ FTIR experiments were conducted and the results are shown in Fig. 9 (FTIR spectra of the $\text{CoCr}_2\text{O}_4\text{-}5$ and $\text{CoCr}_2\text{O}_4\text{-}6$ are shown in Fig. S4 in Supplementary Information). For the $\text{CoCr}_2\text{O}_4\text{-}4$ catalyst (Fig. 9a), after it is exposed to the air + CH_2Cl_2 mixture at 50 °C, bands at 3006, 2985, 2365, 2332, 1610 cm⁻¹ are observed. The bands at 3006 and 2985 cm⁻¹ are attributed to asymmetric vibration (ν_{as}) of $-\text{CH}_2$ group in CH_2Cl_2 molecule [56]; the bands at 2365 and 2332 cm⁻¹ are attributed to gas phase CO_2 ; the band at 1610 cm⁻¹ is assigned to H_2O adsorbed on the catalyst surface, which gradually disappears at elevated temperature. When the catalyst is heated, the bands at 3006 and 2985 cm⁻¹ gradually decline in intensities with increasing temperature, implying either desorption or consumption of the CH_2Cl_2 molecules. Meanwhile, the disappearance of CH_2Cl_2 is accompanied by increasing intensities of the bands at 2365 and 2332 cm⁻¹ (CO_2), and evolution of new bands at 2178, 2120, 1540, 1443 and 1355 cm⁻¹. The weak bands at 2178 and 2120 cm⁻¹ are due to the formation of CO, while the bands at 1540, 1443 and 1355 cm⁻¹ are assigned to asymmetric vibration (ν_{as}), $\delta(\text{CH}_2)$ and symmetric vibration (ν_s) of formate species ($-\text{COOH}$), respectively [4,11,57,58]. Similar observations are also detected on the $\text{CoCr}_2\text{O}_4\text{-}5$ (Fig. S4), $\text{CoCr}_2\text{O}_4\text{-}6$ (Fig. S4) and $\text{CoCr}_2\text{O}_4\text{-}7$ (Fig. 9b) catalysts.

The in situ FTIR results on the CoCr_2O_4 catalysts reflect two facts. One fact is that CH_2Cl_2 oxidation over the spinel CoCr_2O_4 catalyst may follow similar pathways as over Al_2O_3 catalyst [56], with the formate species being the main intermediate. The formate species could be decomposed to CO, which is further oxidized to CO_2 . The other fact is the formation of CO during the reaction. The formation of CO is not detected in the TPSR process (Fig. 5b), its presence is clearly evidenced by the FTIR results (Fig. 9). Although the formation of CO is not desirable in CVOCs oxidation, it may provide a clue of the development of better catalyst system in the future. For example, the spinel oxides could be used as supports for some metals such as Cu and Pt, which are known to be very active in CO oxidation.

To conveniently compare the IR results on these catalysts, normalized intensities of the characteristic bands at 1540 cm⁻¹ (formate species), 2121 cm⁻¹ (CO) and 2356 cm⁻¹ (CO_2) as a function of temperature were plotted and shown in Fig. 10. For each catalyst, the intensity of formate species reaches a maximum at

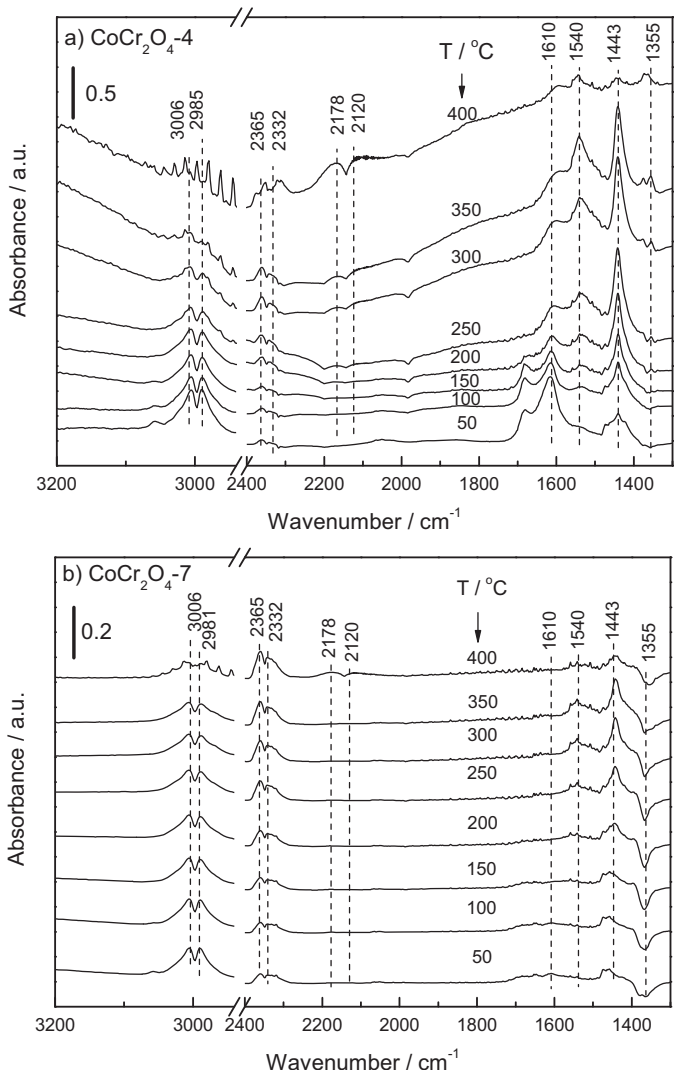


Fig. 9. In situ FTIR spectra of surface reaction of $\text{CH}_2\text{Cl}_2 + \text{air}$ over (a) $\text{CoCr}_2\text{O}_4\text{-}4$ and (b) $\text{CoCr}_2\text{O}_4\text{-}7$ catalysts.

about 350 °C and then declines (Fig. 10a). Meanwhile, the intensities of the bands at 2120 and 2365 cm⁻¹ progressively increase (Fig. 10b and c), and a rapid increase of the intensity is observed at about 350 °C. These results suggests that the formate species could possibly accumulate on the catalyst surface at low temperature, and then be decomposed to CO_x at higher temperature. For the catalysts calcined at different temperatures, the intensities of the bands at 1540 cm⁻¹ (formate species), 2121 cm⁻¹ (CO) and 2356 cm⁻¹ (CO_2) all follow the order of $\text{CoCr}_2\text{O}_4\text{-}4 > \text{CoCr}_2\text{O}_4\text{-}5 > \text{CoCr}_2\text{O}_4\text{-}6 > \text{CoCr}_2\text{O}_4\text{-}7$. This comparison suggests that the $\text{CoCr}_2\text{O}_4\text{-}4$ is more active than the others, which is in good agreement with the overall activities of the catalysts (Fig. 5a).

Based on the FTIR spectra and reported mechanisms of CH_2Cl_2 oxidation over various oxides [56,59], possible reaction pathways of CH_2Cl_2 oxidation over the CoCr_2O_4 catalyst could be demonstrated as shown in Scheme 1. The reaction pathways mainly consist of two sequential cycles: formation of HCHO and oxidation of HCHO to CO and CO_2 . The reaction steps are described as follows:

STEP 1. A CH_2Cl_2 molecule could chemisorb on two adjacent Cr–O sites which serve as acidic sites to form a Cr–OH species and a Cr–OCHCl₂ species.

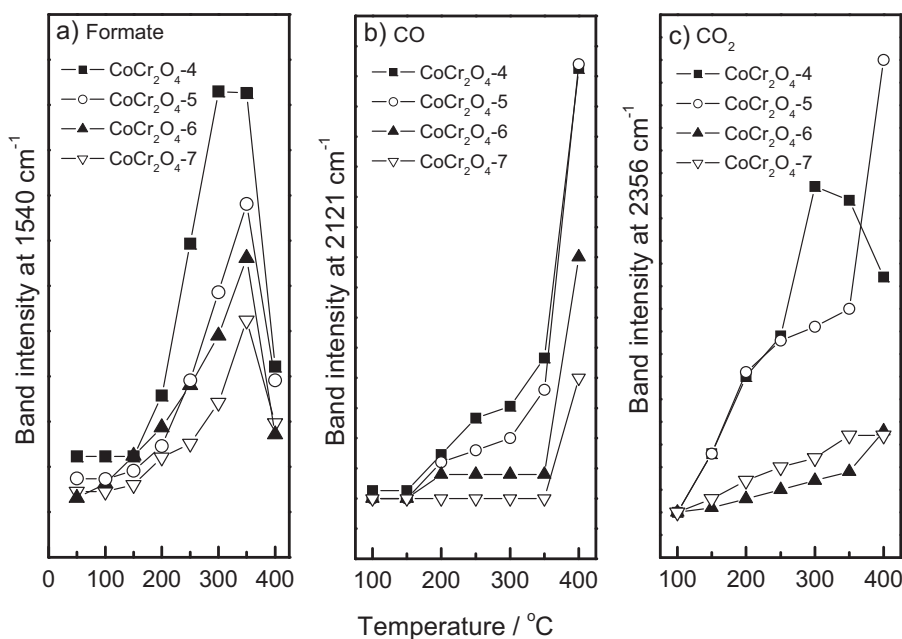
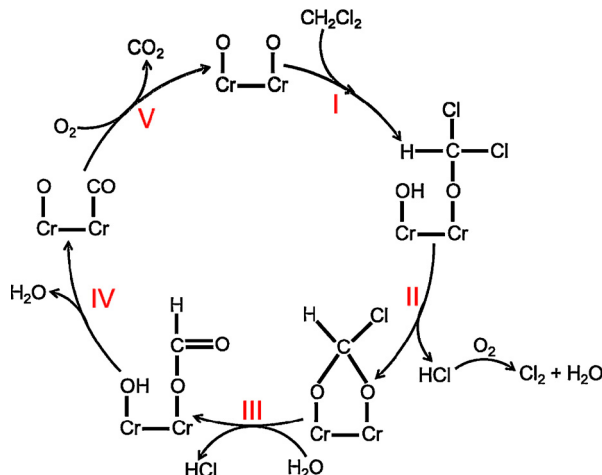


Fig. 10. Intensities of characteristic bands as a function of temperature over different catalysts. (a) Band at 1540 cm⁻¹ (formate species); (b) band at 2121 cm⁻¹ (CO); (c) band at 2356 cm⁻¹ (CO₂).



Scheme 1. Possible reaction pathways of CH₂Cl₂ oxidation over spinel CoCr₂O₄ catalyst.

STEP 2. The Cr–OH and Cr–OCHCl₂ species decompose to HCl and a chloromethoxyl specie (HCO₂Cl). HCl could further react with O₂ via Deacon reaction (2HCl + 1/2 O₂ → Cl₂ + H₂O), which could explain the formation of Cl₂ during the reaction.

STEP 3. The chloromethoxyl specie reacts with H₂O to form a HCl molecule and a Cr–OH and specie a Cr–COOH (formate) specie. Note that H₂O comes from the moisture-containing feed gas. The chloromethoxyl specie could also react with H₂O to form HCl + HCHO molecules. The formation of HCHO is evidenced in TPSR results (Fig. 5b).

STEP 4. The Cr–OH and Cr–COOH species react to form a H₂O molecule and a chemisorbed CO (Cr–CO) and a Cr–O site.

STEP 5. The Cr–CO could further react with O₂ to form a CO₂ molecule and thus complete the reaction cycle.

4. Conclusion

Although spinel type oxides have been widely investigated and CoCr₂O₄ oxide was characterized in detail in literature [30], some new information has been obtained in the current work. Firstly, CoCr₂O₄ catalysts were found to be very active for CH₂Cl₂ oxidation, which has not been reported before. The best catalytic performance is obtained on the catalyst calcined at 400 °C (CoCr₂O₄-4). Secondly, quantitative analyses of the catalytic results in the current work established correlation between the specific reaction rate and some important catalyst properties such as surface area, reducibility and surface acidity. The enhanced activity on this catalyst could be attributed to its highest surface area compared to those calcined at higher temperatures, as it provides more surface acidic sites and active oxygen species than the other catalysts. Thirdly, kinetic study revealed similar activation energies on these catalysts, implying the same reaction pathways of this reaction. Moreover, some reaction intermediates such as formate species have been detected by in situ FTIR, based on which a possible reaction mechanism was proposed.

Acknowledgments

This work is financially supported by Natural Science Foundation of China (Grant No. 21173195).

Appendix A. Supplementary data

Supplementary data associated with this article can be found, in the online version, at <http://dx.doi.org/10.1016/j.apcatb.2014.10.044>.

References

- [1] E.C. Moretti, Practical Solutions for Reducing Volatile Organic Compounds and Hazardous Air Pollutants, Center for Waste Reduction Technologies of the American Institute of Chemical Engineers, New York, 2001.
- [2] J.R. González-Velasco, A. Aranzabal, J.I. Gutiérrez-Ortiz, R. López-Fonseca, M.A. Gutiérrez-Ortiz, Appl. Catal. B: Environ. 19 (1998) 189–197.
- [3] Q.Y. Chen, N. Li, M.F. Luo, J.Q. Lu, Appl. Catal. B: Environ. 127 (2012) 159–166.
- [4] Y. Wang, H.H. Liu, S.Y. Wang, M.F. Luo, J.Q. Lu, J. Catal. 311 (2014) 314–324.

- [5] J.I. Gutiérrez-Ortiz, R. López-Fonseca, U. Aurrekoetxea, J.R. González-Velasco, *J. Catal.* 218 (2003) 148–154.
- [6] B. Chen, C. Bai, R. Cook, J. Wright, C. Wang, *Catal. Today* 30 (1996) 15–20.
- [7] S.X. Chen, Y. Wang, A.P. Jia, H.H. Liu, M.F. Luo, J.Q. Lu, *Appl. Surf. Sci.* 307 (2014) 178–188.
- [8] C. Zhang, W. Hua, C. Wang, Y. Guo, Y. Guo, G. Lu, A. Baylet, A. Giroir-Fendler, *Appl. Catal. B: Environ.* 134–135 (2013) 310–315.
- [9] C. Zhang, C. Wang, W. Zhan, Y. Guo, Y. Guo, G. Lu, A. Baylet, A. Giroir-Fendler, *Appl. Catal. B: Environ.* 129 (2013) 509–516.
- [10] Q. Huang, X. Xue, R. Zhou, *J. Hazard. Mater.* 183 (2010) 694–700.
- [11] L. Pinard, J. Mijoin, P. Magnoux, M. Guisnet, *J. Catal.* 215 (2003) 234–244.
- [12] F. Bertinchamps, C. Grégoire, E.M. Gaigneaux, *Appl. Catal. B: Environ.* 66 (2006) 1–9.
- [13] A.M. Padilla, J. Corella, J.M. Toledo, *Appl. Catal. B: Environ.* 22 (1999) 107–121.
- [14] T. Tanilimış, S. Atalay, H.E. Alpay, F.S. Atalay, *J. Hazard. Mater.* 90 (2002) 157–167.
- [15] H. Rotter, M.V. Landau, M. Herskowitz, *Environ. Sci. Technol.* 39 (2005) 6845–6850.
- [16] S. Krishnamoorthy, J.A. Rivas, M.D. Amiridis, *J. Catal.* 193 (2000) 264–272.
- [17] S.D. Yim, I.-S. Nam, *J. Catal.* 221 (2004) 601–611.
- [18] M. Kang, C.H. Lee, *Appl. Catal. A* 266 (2004) 163–172.
- [19] G.A. Atwood, H.L. Greene, P. Chintawar, R. Rachapudi, B. Ramachandran, C.A. Vogel, *Appl. Catal. B: Environ.* 18 (1998) 51–61.
- [20] S. Kawai, M. Te, *Catal. Today* 44 (1998) 101–109.
- [21] Q. Huang, Z. Meng, R. Zhou, *Appl. Catal. B: Environ.* 115–116 (2012) 179–189.
- [22] R. Rachapudi, P.S. Chintawar, H.L. Greene, *J. Catal.* 185 (1999) 58–72.
- [23] C.F. Windisch, K.F. Ferris, G.J. Exarhos, S.K. Sharma, *Thin Solid Films* 420–421 (2002) 89–99.
- [24] X. Xia, J. Tu, Y. Mai, X. Wang, C. Gu, X.B. Zhao, *ACS Appl. Mater. Interf.* 2 (2010) 186–192.
- [25] M. Burriel, G. Garcia, J. Santiso, A.N. Hansson, S. Linderoth, A. Figueiras, *Thin Solid Films* 473 (2005) 98–103.
- [26] A.G. Avila, E.C. Barrera, L.A. Huerta, S. Muhl, *Sol. Energy Mater. Sol. Cells* 82 (2004) 269–278.
- [27] M. Ando, T. Kobayashi, M. Haruta, *Sens. Actuators B* 32 (1996) 157–160.
- [28] L.C. Schumacher, I.B. Holzhueter, I.R. Hill, M.J. Dignam, *Electrochim. Acta* 35 (1990) 975–984.
- [29] J. Chen, Y. Zhang, H. Arandiyani, *Catal. Today* 201 (2013) 12–18.
- [30] D.C. Kim, S.K. Ihm, *Environ. Sci. Technol.* 35 (2001) 222–226.
- [31] J. Chen, W. Shi, X. Zhang, *Environ. Sci. Technol.* 45 (2011) 8491–8947.
- [32] H.S. Fogler, *Elements of Chemical Reaction Engineering*, 4th Ed., Pearson Education Inc., 2006, pp. 839.
- [33] G.L. Castiglioni, G. Minelli, P. Porta, A. Vaccari, *J. Solid State Chem.* 152 (2000) 526–532.
- [34] W.B. White, B.A. Deangelis, *Spectrochim. Acta A* 23 (1967) 985–995.
- [35] C. Suchomski, C. Reitz, K. Brezesinski, *Chem. Mater.* 24 (2011) 155–165.
- [36] J. Chen, W. Shi, S. Yang, *J. Phys. Chem. C* 115 (2011) 17400–17408.
- [37] M. Maczka, M. Ptak, M. Kurnatowska, J. Hanuza, *Mater. Chem. Phys.* 138 (2013) 682–688.
- [38] P. Chandromohan, M.P. Srinivasan, S. Velmurugan, *J. Solid State Chem.* 184 (2011) 89–96.
- [39] G.C. Allen, S.J. Harris, L.A. Jutson, *Appl. Surf. Sci.* 37 (1989) 111–134.
- [40] N.S. McIntyre, M.G. Cook, *Anal. Chem.* 47 (1975) 2208–2213.
- [41] W. Wei, W. Chen, D.G. Ivey, *Chem. Mater.* 20 (2008) 1941–1947.
- [42] Y. Lin, W. Cai, X. Tian, X. Liu, G. Wang, C. Liang, *J. Mater. Chem.* 21 (2011) 991–997.
- [43] X. Xie, Y. Li, Z. Liu, M. Haruta, W. Shen, *Nature* 458 (2009) 746–749.
- [44] J.P. Jacobs, A. Maltha, J.R.H. Reintjes, T. Drimal, V. Ponec, H.H. Brongersma, *J. Catal.* 147 (1994) 294–300.
- [45] J. Słoczyński, J. Janas, T. Machej, J. Rynkowski, J. Stoch, *Appl. Catal. B: Environ.* 24 (2000) 45–60.
- [46] K. Rida, A. Benabbas, F. Bouremmad, M.A. Pena, A. Martinez-Arias, *Appl. Catal. A* 375 (2010) 101–106.
- [47] A. La Rosa-Toro, R. Berenguer, C. Quijada, F. Montilla, E. Morallón, J.L. Vazquez, *J. Phys. Chem. B* 110 (2006) 24021–24029.
- [48] J. Li, X. Liang, S. Xu, J. Hao, *Appl. Catal. B: Environ.* 90 (2009) 307–312.
- [49] Y. Wang, Z. Zhou, M. Jia, X. Zhu, *Catal. Lett.* 104 (2005) 67–71.
- [50] B. de Rivas, R. López-Fonseca, C. Jiménez-González, *J. Catal.* 281 (2011) 88–97.
- [51] P. Zimmer, A. Tschope, R. Birringer, *J. Catal.* 205 (2002) 339–345.
- [52] S.C. Petrosius, R.S. Drago, V. Young, G.C. Grunewald, *J. Am. Chem. Soc.* 115 (1993) 6131–6137.
- [53] J.I. Gutiérrez-Ortiz, R. López-Fonseca, U. Aurrekoetxea, J.R. González-Velasco, *J. Catal.* 218 (2003) 148–154.
- [54] L. Jin, R. Ma, J. Lin, L. Meng, Y. Wang, M. Luo, *Ind. Eng. Chem. Res.* 50 (2011) 10878–10882.
- [55] R. Ma, P. Hu, L. Jin, Y. Wang, J. Lu, M. Luo, *Catal. Today* 175 (2011) 598–602.
- [56] I. Maupin, L. Pinard, J. Mijion, P. Magnoux, *J. Catal.* 291 (2012) 104–109.
- [57] C. Zhang, H. He, K. Tanaka, *Appl. Catal. B: Environ.* 65 (2006) 37–43.
- [58] R. Yang, L. Fu, Y. Zhang, N. Tsubaki, *J. Catal.* 228 (2004) 23–35.
- [59] B. Ramachandran, H.L. Greene, S. Chatterjee, *Appl. Catal. B* 8 (1996) 157–182.